LA-9413-MS

Los Alamos National Laboratory is operated by the University of California for the United States Department of Energy under contract W-7405-ENG-36.

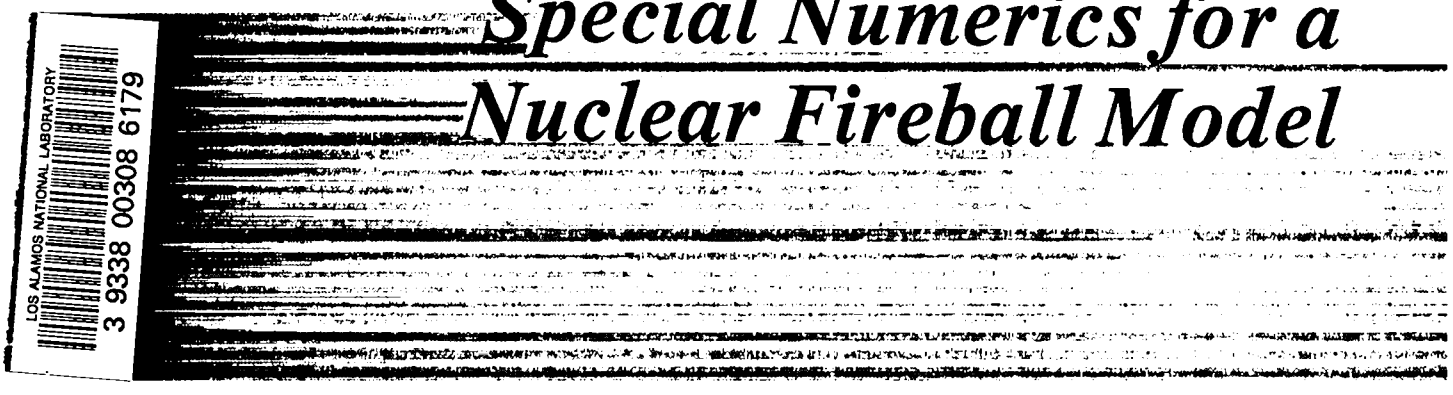

Special Numerics for a Nuclear Fireball Model

Los Alamos National Laboratory
Los Alamos, New Mexico 87545

Edited by Glenda Ponder, Group ESS-4

LA-9413-MS

UC-34
Issued: June 1982

Special Numerics for a Nuclear Fireball Model

J. Zinn
C. D. Sutherland

6403
6949

Los Alamos National Laboratory
Los Alamos, New Mexico 87545

SPECIAL NUMERICS FOR A NUCLEAR FIREBALL MODEL

by

J. Zinn and C. D. Sutherland

ABSTRACT

This report describes recent advances in techniques for controlling oscillations and numerical errors in the computation of radiant power emitted by a nuclear fireball. The oscillations and the errors come from the use of a numerical mesh that is orders of magnitude coarser than the physical dimensions of fireball surface structures that determine the brightness.

INTRODUCTION

Several years ago we set ourselves the task of learning to make a legitimate first-principles computation of the first pulse of the radiant power versus time curve of a sea level nuclear fireball. The purpose was primarily to see what diagnostic information could be extracted from optical data from atmospheric nuclear tests. One requirement was to include the nonequilibrium chemistry effects that are involved with what we have called "smog." Another requirement was to eliminate the persistent bad numerical problems that occur in fireball codes as the result of trying to compute radiative outputs from structures whose physical dimensions are orders of magnitude smaller than the smallest numerical mesh sizes that one can use in a practical fireball computation.

This report describes our approach to solving the oscillation problems. The chemistry will be discussed in a later report.

THE ELIMINATION OF OSCILLATIONS IN COMPUTED RADIANT POWER

The reference fireball computer code, for the purpose of this discussion, is our local code, known as "RADFLO."[1] Figure 1 is a plot from a "raw" computation of computed visible power output from a 1-Mt fireball during the first thermal pulse. We have used the standard RADFLO radiation transport algorithm throughout the mesh with no special smoothing algorithms across the front. The computed power exhibits a large but quite regular oscillation. One can note a change in the pattern at 100 to 300 μs when the fireball expansion is changing from radiative to hydrodynamic. "First maximum" is at about 1.3 ms.

These oscillations come from the use, by necessity, of a computational mesh that is orders of magnitude coarser than the intrinsic thickness of the fireball radiating surface. (The mesh spacings in this problem are about 150 cm; a typical fireball shock front thickness is 1 mm). This might not be a problem were it not for the extreme temperature dependence of the optical absorption coefficient of air, such that a moderately thick layer becomes opaque before it becomes very luminous.

It is a fundamental assumption in a finite difference computation that each finite mesh cell has a definite temperature that is constant across the cell. Thus,in effect,a smoothly varying temperature profile is approximated by a stepwise-varying profile. Also the propagation of an ideal step-function thermal wave moving from left to right through the mesh is represented numerically by a process where at each instant of time the temperature step is distributed over two or more cells. A cell at the instantaneous front of the wave heats up in stepwise fashion until it attains the final-wave temperature. Then the next successive cell begins to heat up step by step, and so on. If the step function thermal wave is in air, then each intermediate temperature cell, as it heats up, becomes more and more opaque, absorbing more and more of the light from the hotter cells behind. This causes the transmitted light intensity to drop, at first, until that cell becomes hot enough to emit more light than it transmits. The light crossing the front then increases until that cell reaches the final wave temperature. Then the next cell begins to heat up, and the light intensity begins to decrease again, and so on. The process is illustrated in Fig. 2, which shows a time-sequence of five computed temperature profiles for a restricted region near the front from an actual

computation of a propagating thermal wave. Also shown for each cell is the instantaneous cell optical thickness, τ, for a typical wavelength in the green. Shown also for each of the five "snapshots" is the computed emergent green light intensity for the direction normal to the front. In this sequence the emergent intensity is determined almost entirely by the cells labelled 1, 2, and 3, and it is described to good approximation by the expression

$$I = [B_1(1-e^{-\tau}1)e^{-\tau}2 + B_2(1-e^{-\tau}2)]\ e^{-\tau}3 + B_3(1-e^{-\tau}3). \qquad (1)$$

Here B_i means the blackbody intensity in the green frequency group in cell i, and τ_i is the cell optical thickness for green light.

In the sequence shown, τ_1 is large throughout. In the first frame (at 43 μs) τ_2 and τ_3 are both small, so the first term is dominant, and almost the entire contribution to the intensity I comes from cell 1. In the second frame (at 44 μs) τ_2 has increased significantly, while B_2 is still small. The intensity has decreased drastically. The contributions of cells 1 and 2 to I are now about equal. In the third frame (at 50 μs) τ_2 has increased further, but B_2 has also increased (while τ_3 and B_3 remain small). The main contribution to I now comes from cell 2, and I is increasing as its temperature increases. In frame 4 (at 62 μs), τ_2 and B_2 have increased further, while τ_3 and B_3 are still small. The intensity has increased to a new maximum. The main contribution is still from cell 2. In frame 5 (at 63 μs), τ_3 has increased significantly; cell 3 has become a very strong attenuator, and I has dropped to a new minimum. This kind of sequence repeats over and over again, resulting in a quite regular sawtooth oscillation in I. The very abrupt intensity drops occur at those times when a cell at the front has a temperature between 6000 and 9000 K, where the free electron bremsstrahlung absorption coefficient increases rapidly.

The frequency of the oscillation can be increased by decreasing the cell thicknesses. However, the amplitude remains large as long as the cell thickness is larger than the intrinsic thickness of the wave front, which is a few millimeters [1,2,3] (See Appendix.) The cell thicknesses in this example are 150 cm.

The oscillation problem persists throughout the radiative fireball expansion phase. It continues into the hydrodynamic expansion phase.

However, in the hydrodynamic phase it is modified and exacerbated by the effects of the artificial viscous pressure, a device that we use for smoothing the computed profiles of state variables across the shock. The artificial PV work performed ahead of the shock by the action of the viscous pressure produces a heated toe that absorbs light emitted by the shock. This causes the computed shock luminosity to be generally smaller than it should be, while at the same time oscillating for the reasons that we have just described.

The differential equation for the internal energy per unit volume, E, in a moving fluid element can be written as

$$\frac{dE}{dt} = - P\nabla\cdot\vec{v} - \nabla\cdot\vec{F} \qquad (2)$$

where P is the pressure, $\vec{v}$ the velocity, and $\vec{F}$ the radiation flux (integrated over all frequencies). The artivicial viscous pressure, Q, when it is introduced, is simply added to P, so the hydrodynamic work term in Eq. (2) becomes $(P+Q)\nabla\cdot\vec{v}$.

The algorithm for the viscous pressure, Q, is such that Q = 0 in regions that are expanding (i.e., behind the shock front). When this is the case it can be shown that the shock temperature will be correctly computed i.e., it will be the same as the value given by the Rankine-Hugoniot relation with no viscous pressure. This is obviously a nice property and it leads us to a numerical algorithm by which we can get rid of both the optical power oscillation and the optical attenuation produced by the artificial preshock viscous toe. We proceed as follows: For each numerical cell we use two separate energy variables $E_1(r,t)$ and $E_2(r,t)$ instead of just one. Variable E_1 is the "normal" computed energy, whose computed value is advanced from one time step to the next with the inclusion of all terms in Eq. (2); i.e., with the hydrodynamic PV and QV work terms as well as the terms arising from radiative energy transport. The pressure P is computed from the equation of state as $P(\rho,E_1)$. Thus the hydrodynamic portion of the computation is run in the customary way. The second energy variable E_2 is advanced in time using the radiative transport terms only; however in regions that are expanding, such that Q = 0, E_2 is set equal to E_1. As a result E_2 looks like a good step function, whose postshock value agrees with the Rankine-Hugoniot relations, and whose

preshock values reflect the effects of radiative transport but contain no artificial quasi-hydrodynamic effects. The temperature is computed from the equation of state as $T(\rho,E_2)$. The temperature is the quantity used in the radiative transport part of the computation for generating Planck functions and absorption coefficients. Thus in this way the radiation transport computation is cleansed of the bad effects of viscous pressure. Since the algorithm for E_2 is such that it is a good step function at the shock front, and T is as well, the computed power emitted by the shock does not tend to oscillate. Moreover, we have been able to show that it has the correct value, as long as the shock velocity is not so large that its luminosity is less than that of a blackbody -- i.e., there is no attenuating radiative precursor.[2,3] (See Appendix.)

When the shock velocity exceeds 35 km/s (in air of sea level density) the luminosity computed with the above algorithm is too large. For this problem we need another algorithm, which is described below. This algorithm will also eliminate (or at least reduce) the oscillations in computed power during the radiative thermal-wave phase of fireball development. We proceed as follows:

1. First we maintain a running computation of the fireball expansion velocity. This velocity is defined as the numerical time derivative of the outermost radial locus of T = 2 eV. If this velocity is less than 35 km/s, we do nothing special. If it exceeds 35 km/s we proceed to steps 2 and 3.
2. The separate steady-state shock and thermal-wave computations of Zinn and Sutherland[2] lead to a definition of an effective radiating temperature $T_{eff}(D)$, applicable to photon energies below 6.5 eV (where D is the wave velocity). A plot of T_{eff} vs D is shown in Fig. 3. When D >35 km/s the fireball surface is assumed to radiate as a blackbody with the appropriate effective temperature from Fig. 3 (for $h\nu$ <6.5 eV), attenuated by any diffuse absorbing region (x-ray veil and smog) that may lie outside the front. This requires the insertion of a special patch in place of the normal transport algorithm at the appropriate place. To do this we first look up the values of the Planckian $B_\nu(T_{eff},\nu)$ by interpolation from the existing stored table of $B_\nu(T,\nu)$ vs T. Next, we must find the correct location for the patch.

3. Starting from the outer edge of the mesh and stepping inward, we look for the outermost cell that has a temperature exceeding 20 eV. The serial index of this cell will be called i. The outer boundary of this cell is R_{i+1}. The patch will be applied at R_{i+2}. We next compute the precise radius of the front, R_{FB}, defined as the interpolated locus of $T \approx 20$ eV. Between R_{FB} and the location of the patch, R_{i+2}, is an attenuating layer of thickness $\Delta R_L = R_{i+2} - R_{FB}$. We interpolate a temperature for the midpoint of this layer from the temperatures of cells i+1 and i+2, find the corresponding opacity κ from the stored opacity tables and compute the optical thickness $\tau = \kappa\rho\Delta R_L$. Finally the patched outward radiant flux F_ν^+ at R_{i+2} is given by

$$2\pi(R_{FB}/R_{i+2})^2 B_\nu(T_{eff},\nu)E_3(\tau) , \tag{3}$$

where $E_3(\tau)$ is the third exponential integral function:

$$E_3(\tau) = \int_1^\infty \frac{e^{-\tau x}}{x^3}\,dx \tag{4}$$

The power computed with this algorithm has very little tendency to oscillate, since the temperature of the cell outside R_{i+2} is not much affected by the approaching front. If there are attenuation terms arising from cells outside R_{i+2}, they are taken into account in the normal way with the normal (RADFLO) algorithm.

We are of course begging the question: "Is the surface structure of a dynamically varying shock wave (or thermal wave) similar to that of a steady shock (or thermal wave) with the same instantaneous velocity?" We do not have a complete answer to this question. In the case of well-developed shock waves, as they are modeled by RADFLO, the postshock temperatures are indeed found to agree with the Rankine-Hugoniot temperatures computed for steady shock waves of the same velocity. Moreover, the time required for the radiative precursor to form, or to change in response to a change in shock velocity, is extremely short (or

order $10^9 l/T^3$, where l is the precursor thickness and T is the shock temperature. For a 20 eV shock with a 0.5 mm precursor this time is about 4 ns). A similarly short time should be required for adjustment of the front of a thermal wave. Therefore, shock waves or thermal waves whose velocities vary slowly on a time scale of microseconds should have surface structures similar to steady waves. Less can be said about transitional wavefront structures that occur during the development of a shock wave out of a decaying thermal wave.

Apart from these two modifications just described, the radiation and hydrodynamics portions of RADFLO are as they have been for years.[1,4]

With the new modifications the code produces much better computations of fireball radiant power output. They are better in the sense that they now produce an accurate numerical representation of the physics that is in the model. It is interesting to note that the radiant power that we now compute is larger than that represented by the upper envelope of the power oscillations that one would compute with the original unmodified code.

III. SAMPLE CASES

We do not intend in this report to compare any computations with experimental data. We will however show two computations. Figure 4 is a computation of radiant power versus time for a generic 1-Mt explosion at sea level altitude. The power is calculated for the spectral bandpass of an unfiltered silicon photodetector. Figure 5 is the equivalent power-time curve for a 20-kt explosion.

The megaton computation shown in Fig. 4 starts from the same set of input parameters as the oscillating computation in Fig. 1; therefore, the results are directly comparable. One will note that the visible power at first maximum is considerably larger in Fig. 5 (5×10^{14} W) than the highest point on the upper envelope of the oscillations in Fig. 1 (1.5×10^{14} W). The reason is that in Fig. 1 the artificial viscous precursor is causing significant attenuation even at the maxima in the oscillating power.

Now that the power oscillations and viscous pressure problems are reduced, it is possible, to a limited extent, to resolve in the computation the transition from radiative fireball growth to hydrodynamic growth. For this purpose it is helpful to reduce the artificial viscous pressure as far

as possible, i.e., to a level where hydrodynamic oscillations behind the shock become noticeable but not enough to produce severe oscillations in the shock front temperature (or brightness).

In the megaton computation the transition from radiative to hydrodynamic expansion extends over a period between about 150 and 400 μs. During this time the shock-front density ratio grows from 2.4 to 9.2. The fireball radius grows from 52 to 62 m (through 5 mesh cells), and the expansion velocity drops from 61 to 32 km/s. The radiant power algorithm changes when the velocity is 35 km/s (as described in the previous section), and this occurs at 340 μs. One can see the effect of this transition in Fig. 4. The oscillations after 340 μs occur because of the small viscous pressure that we chose to use. They can be eliminated by increasing the viscous pressure, but with some loss of resolution of the radiative-to-hydrodynamic transition.

With the oscillations reduced, more credence can be given to small inflections in the power-time curve, such as the one that occurs at 0.01 to 0.02 s in Fig. 4. We have seen these inflections for many years, both in the computations and in fireball data. They occur when the shock temperature is about 0.8 eV, and are caused by the sharp decrease in effective specific heat with decreasing temperature in that region of the air equation of state. This was first pointed out by D. Sappenfield.

These computations do not include nonequilibrium chemistry. That subject will be discussed in a later report. The radiative absorption coefficients used in the transport computation are those of air in an assumed state of local thermodynamic equilibrium. It is well known that the air outside the fireball during its early development is far out of chemical equilibrium, and computations that are based on local thermodynamic equilibrium do not agree very well with nuclear test data.

Figure 5 is a plot of the computed radiant power versus time for a generic 20-kt sea level explosion, again for the spectral bandpass of a silicon detector. In this generic case most of the bomb yield appears initially as kinetic and internal energy of the vaporized bomb materials, and not much energy is radiated as x rays. Therefore no x-ray veil is developed and there is no clearly defined radiative phase of fireball expansion. The expanding bomb gases produce an intense shock wave with 200 km/s velocity, which generates a radiative expansion ahead of it; however

the numerical mesh is too coarse (ca 1-m cells) to separate the radiative precursor from the shock. The steady thermal-wave algorithm is used to compute the brightness of the structure until its velocity drops below 35 km/s. That transition occurs at 197 μs. The computed radiant power maximum occurs at 170 μs when the computed velocity is 45 km/s. That velocity is close to, but not exactly equal to, 48 km/s, the value for which the effective temperature of a steady shock is maximum (see Fig. 3). It is no surprise that the brightness of the shock, as controlled by its radiative precursor, has a dominant influence on the shape of the radiant power-time curve.

This computation shows a pronounced radiant power shelf at 3.5 to 4 ms. As in the 1 Mt case this comes from the tendency of the shock temperature to hold at about 0.8 eV, despite the rapid drop in shock velocity and internal energy.

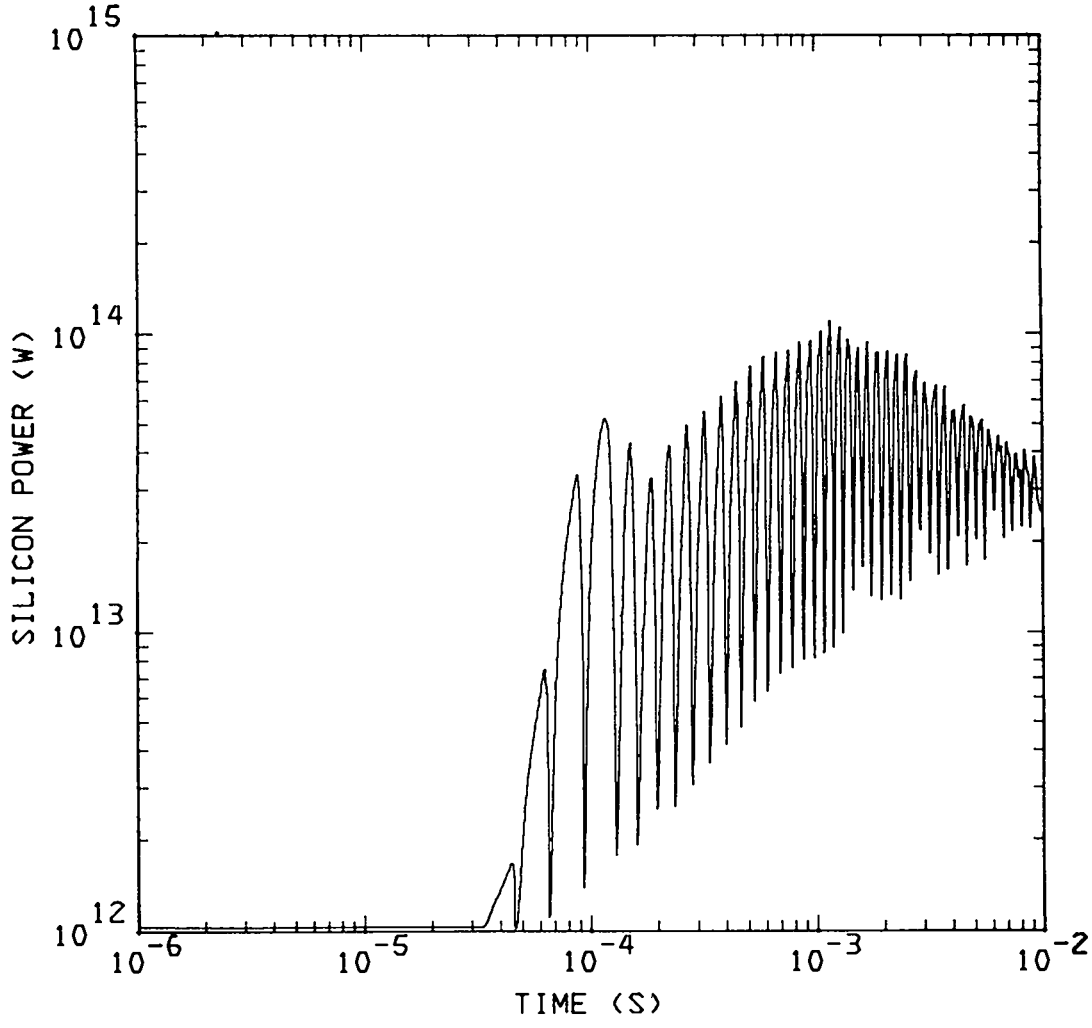

Fig. 1.

A plot of computed visible radiant power vs time for a generic 1-Mt explosion, from a "raw" computation where no special algorithms to remove oscillations were used. Every numerical time step is plotted.

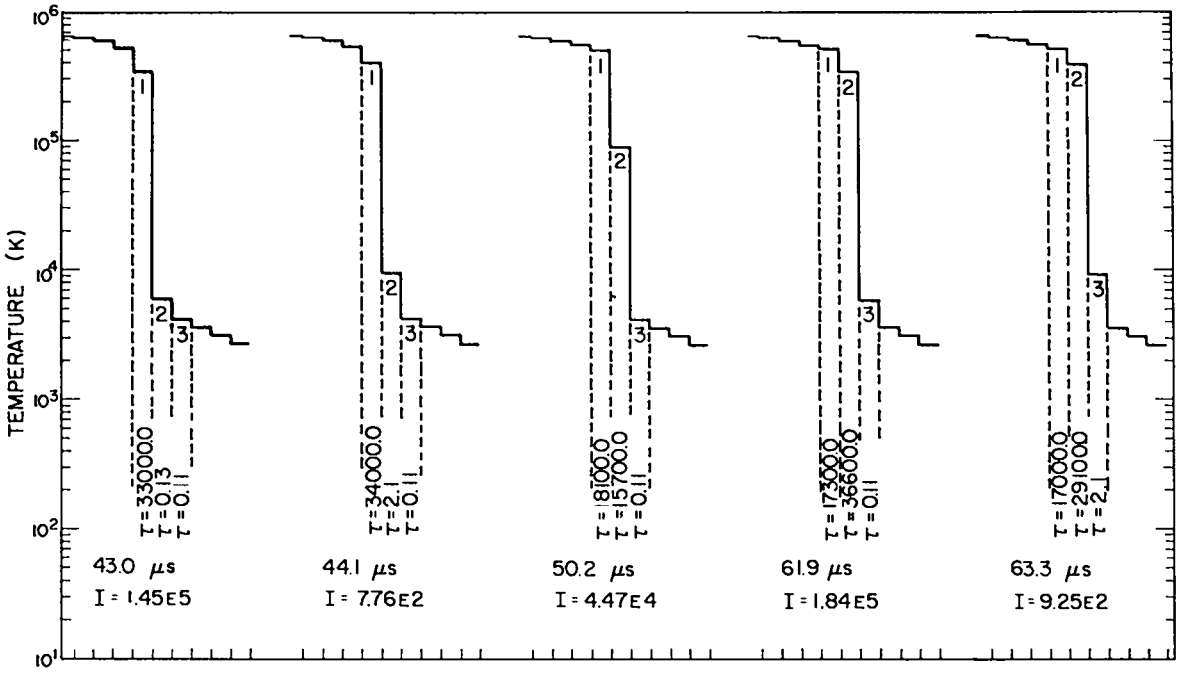

Fig. 2.

A sequence of five computed temperature profiles showing stepwise radiative expansion of the fireball in another megaton computation. Also shown are the computed intensities of green light emergent from the fireball surface at the selected times. (These are not consecutive time steps in the computation. They are selected times to illustrate the intensity oscillation.) The intensity is determined mainly by the three cells labeled 1, 2, 3. The optical thicknesses of cells 1, 2, 3 are shown at each of the selected times.

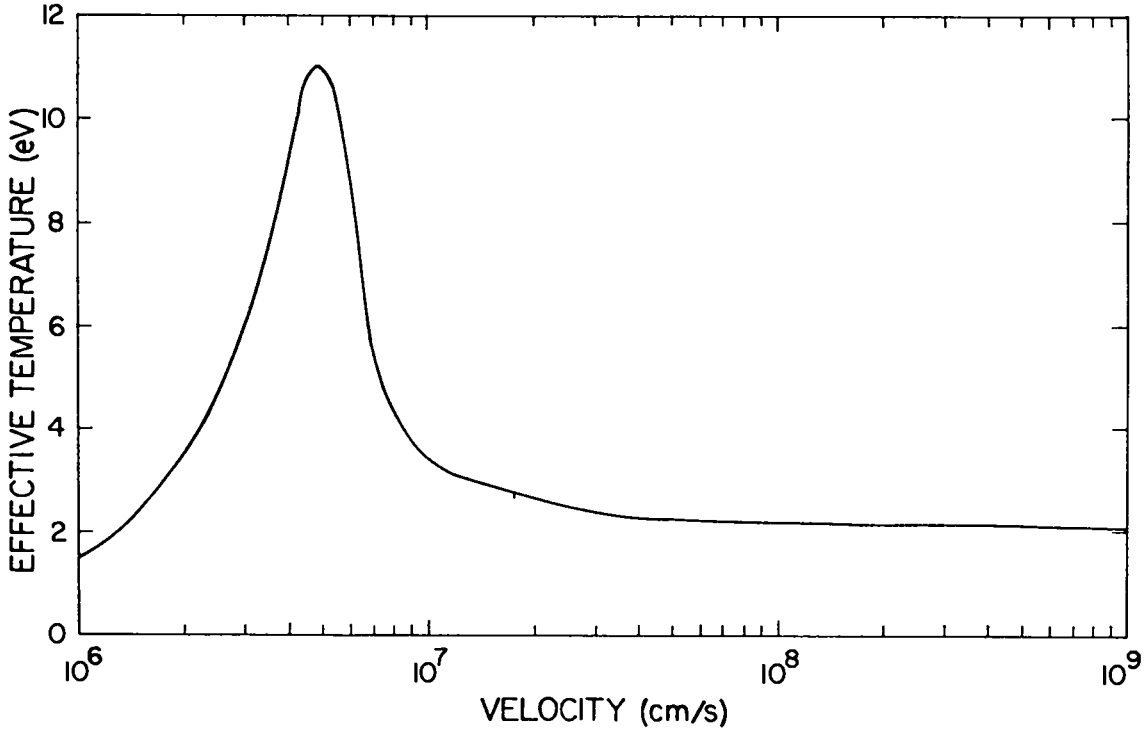

Fig. 3.

Computed effective radiating temperature vs wavefront velocity for shock waves and thermal waves in sea level air (effective temperature for visible radiation).

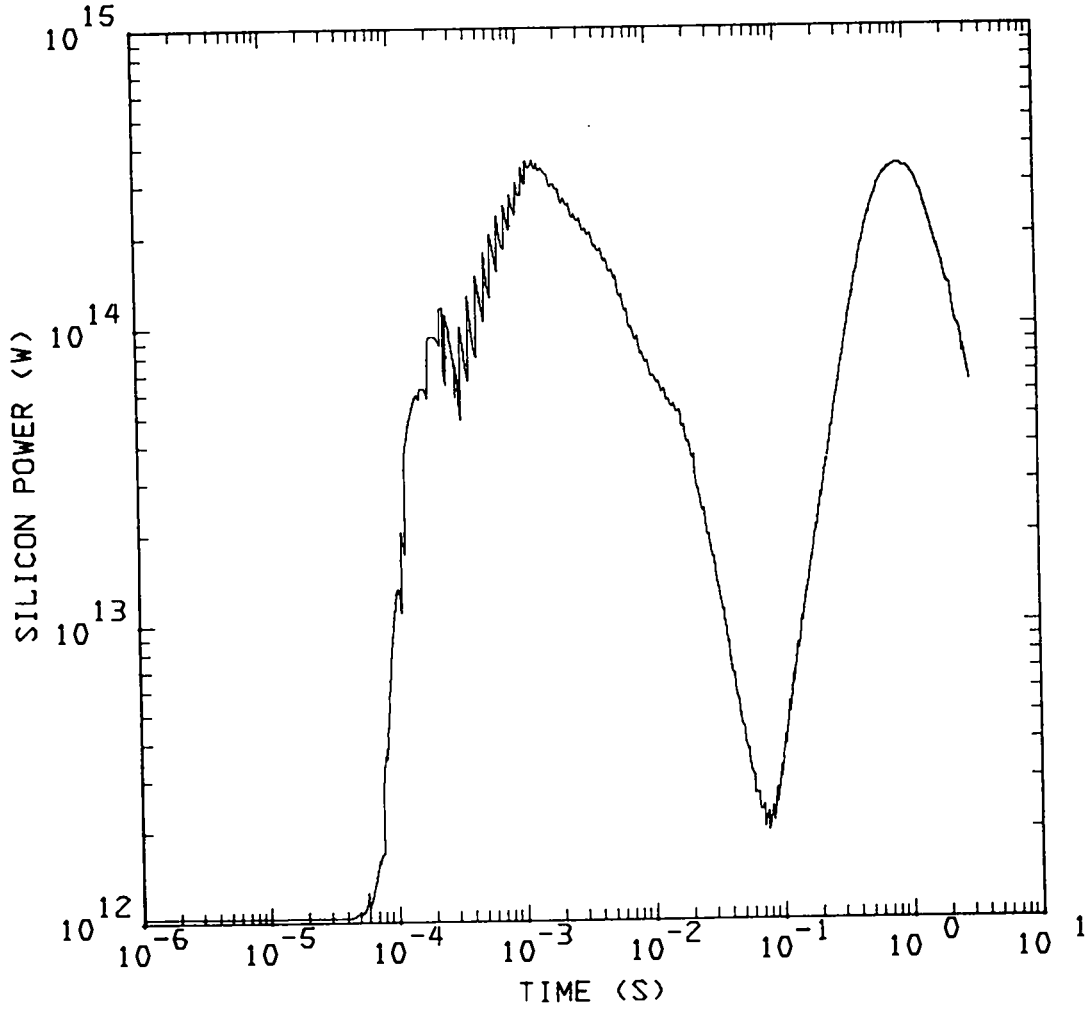

Fig. 4.

Computed radiant power vs time for a generic megaton sea level fireball as integrated over the spectral bandpass of a silicon photodetector. The oscillation-removal algorithms were used for this computation.

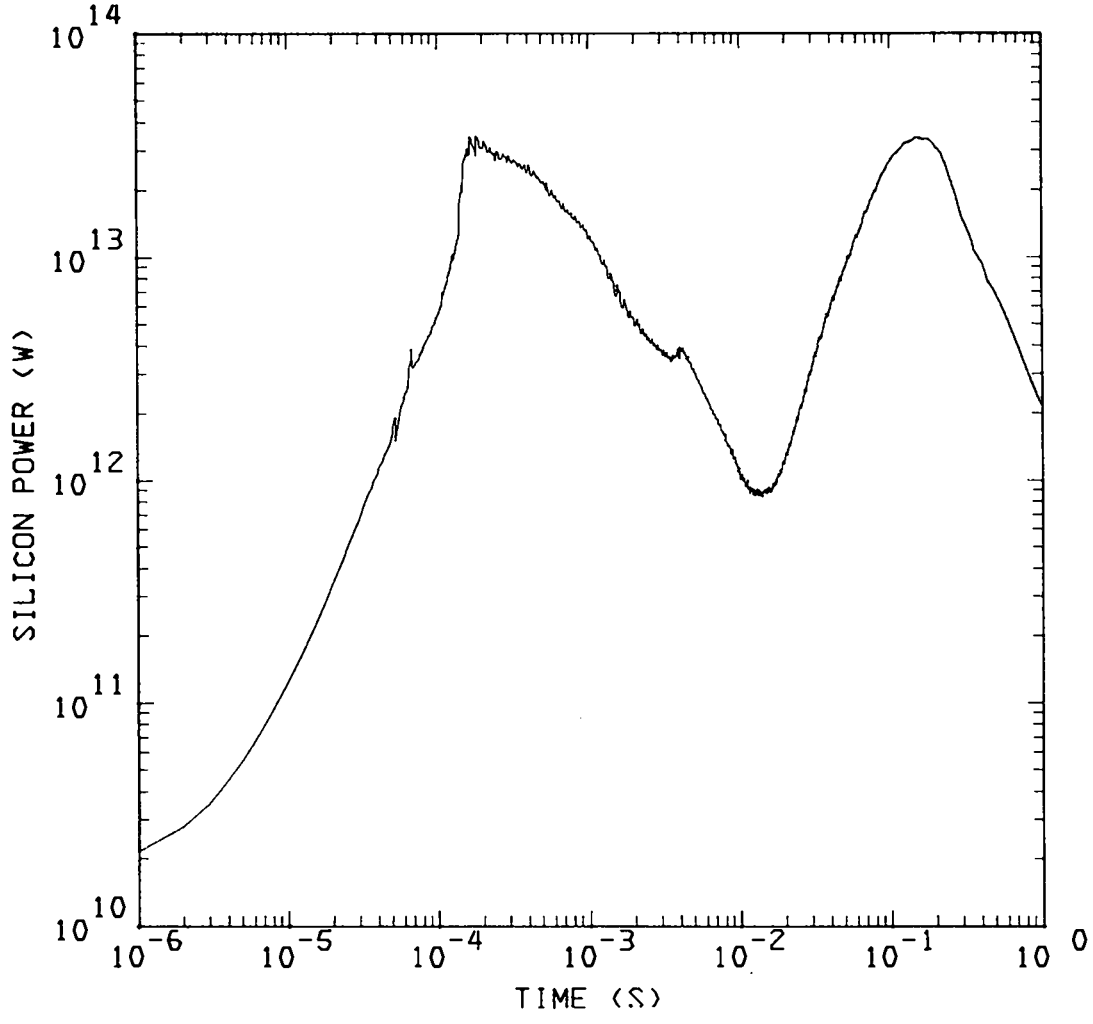

Fig. 5.

Computed radiant power vs time for a 20-kt explosion as integrated over the spectral bandpass of a silicon photodetector. The oscillation-removal algorithms were used for this computation.

APPENDIX

STRUCTURE AND LUMINOSITY OF STEADY THERMAL WAVES AND SHOCK WAVES

Because of the coarse mesh used in RADFLO and other fireball codes, they are not able to compute the detailed thermal structure of the fireball surface or its optical luminosity. To compute those things we had to develop an entirely separate model, which is based on the assumption of a steady state of propagation in a 1D coordinate system that moves at the velocity of the wave front.[2,3] Under those circumstances all time derivatives can be replaced by spatial derivatives, and mesh cell widths can be made arbitrarily small. We used 10^{-2} cm cells.

The equations are those of hydrodynamics and radiation transport, assuming local thermodynamic equilibrium and steady state in the moving coordinate system, whose velocity (D) is specified. A tabular equation of state and tabular equilibrium opacities are included, the same ones that are used in RADFLO. The equations are

$$\rho(D-v) = \rho_o D \quad \text{(cons. of mass)}, \tag{A-1}$$

$$\rho_o Dv = P - P_o + 1/3\, aT^4 \quad \text{(cons. of momentum)}, \tag{A-2}$$

and

$$\rho_o D\left(E + \frac{aT^4}{\rho} - E_o\right) = Pv - \frac{1}{2}\rho_o Dv^2 + F \quad \text{(cons. of energy)}, \tag{A-3}$$

where ρ, E, T, P, v and F are, respectively, the mass density, material specific internal energy, temperature, pressure, fluid velocity (in laboratory coordinates), and the total radiation flux. Subscript zero refers to conditions far ahead of the front. The values of v and F far ahead of the front are assumed to be zero.

The flux F(x) at position x is defined by

$$F = \int_0^\infty F_\nu \, d\nu = 2\pi \int_0^\infty d\nu \int_0^\infty I_\nu(\nu,\theta,x) \sin\theta \cos\theta \, d\theta, \tag{A-4}$$

where I_ν is the specific radiation intensity at position x, angle θ, and frequency ν. Under conditions of local thermodynamic equilibrium, the spatial variation if I_ν is described by the transport equation

$$\frac{dI_\nu}{dx} = \mu'(B_\nu - I_\nu)/\cos\theta, \tag{A-5}$$

or the equivalent integral form,

$$I_\nu(\nu,\theta,x) = I_\nu(\nu,\theta,0)\ \exp\left(-\int_0^x \mu' dx/\cos\theta\right)$$

$$+ \int_0^x \mu' B_\nu \exp\left(-\int_{x'}^x \mu' dx''/\cos\theta\right) dx'/\cos\theta, \tag{A-6}$$

where μ' is the absorption coefficient corrected for stimulated emission, and B_ν is the Planck function. Both μ' and B_ν are functions of ν and x.

The assumed boundary conditions are: (1) far ahead of the wave front $I_\nu(\nu,\theta) = 0$ for all θ and all ν, and (2) far behind the wave front the values of $I_\nu(\nu,\theta)$ are prescribed.

Further details are described in Ref. 2, which are not included here. Some results are shown in Figs. A-1, A-2, and A-3. Figures A-1, and A-2 show temperature profiles of shock waves and thermal waves with velocities between 30 and 10^4 km/s in normal sea level density air. Figure A-3, a plot of visible luminosity as a function of propagation velocity, shows that the computed luminosity of a shock whose velocity is less than 35 km/s is the same as that of a blackbody whose temperature is the Rankine-Hugoniot temperature. For higher velocities the brightnesses are much smaller. The diminished brightness is caused by a precursor toe on the temperature profile, caused by the transport of uv radiation ahead of the shock. The toe is hot and thick enough to attenuate the radiation coming through it.

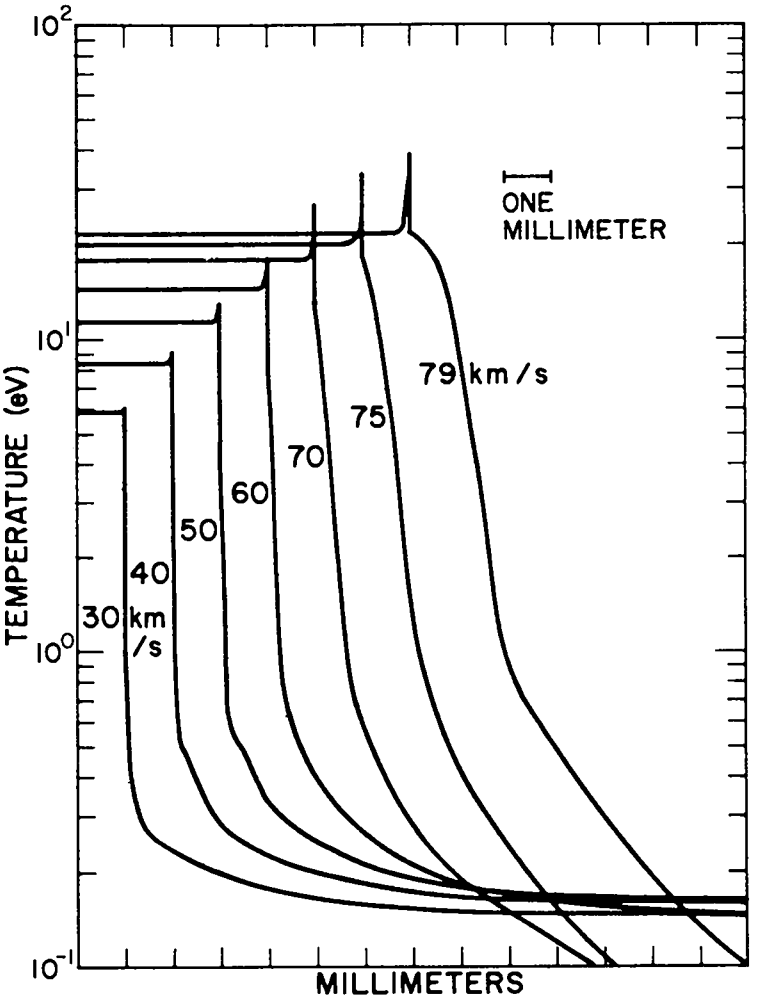

Fig. A-1.
Composite plot of computed temperature profiles for high-velocity shock waves with several different velocities (in air of normal sea level density).

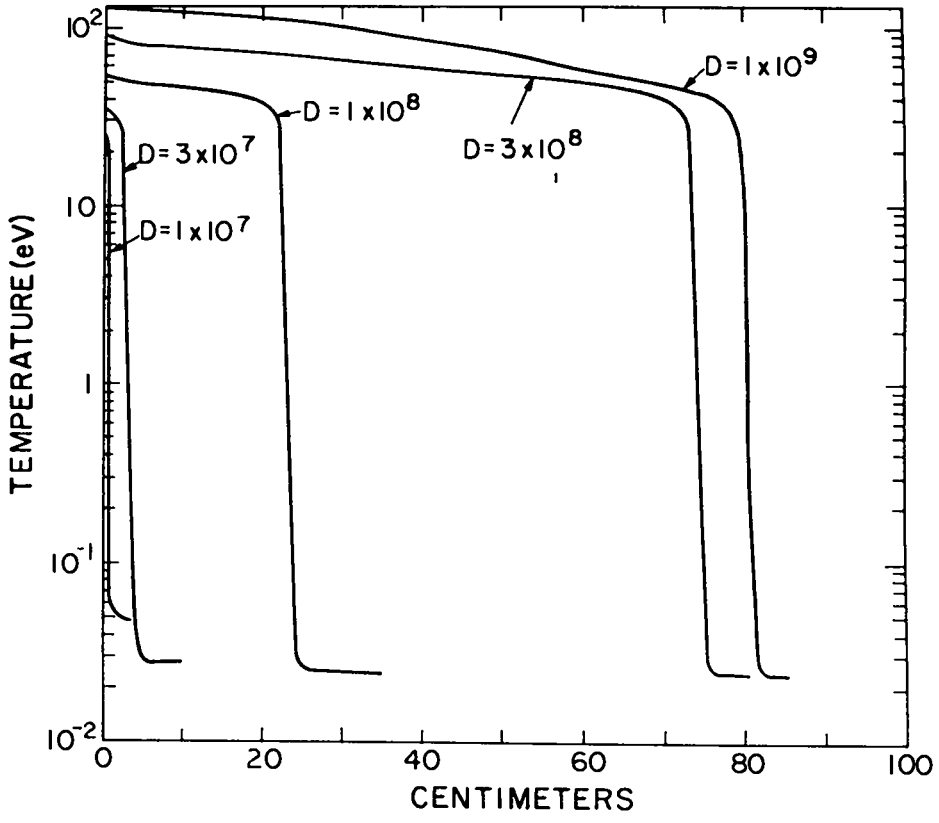

Fig. A-2.

Composite plot of computed temperature profiles of thermal waves with velocities between 100 and 10^4 km/s (in normal density air).

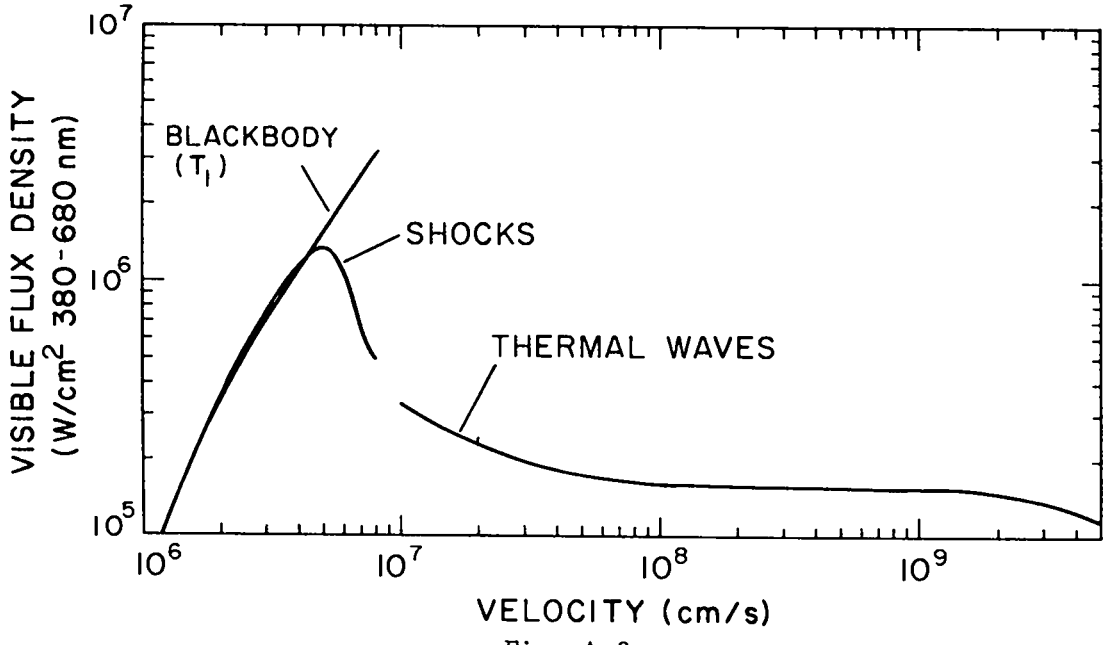

Fig. A-3.

Visible flux density (W/cm^2 s 380-680 nm) for shock waves and thermal waves as a function of propagation velocity (in normal density air).

REFERENCES

1. John Zinn, "A Finite Difference Scheme for Time-Dependent Spherical Radiation Hydrodynamics Problems," J. Comp. Phys., 13, 569-590 (1973).

2. J. Zinn and C. D. Sutherland, "Structure and Luminosity of Radiative Thermal Waves in Air," submitted to The Physics of Fluids, June 1981.

3. J. Zinn and R. C. Anderson, "Structure and Luminosity of Strong Shock Waves in Air," The Physics of Fluids, 16, 1639-1644 (1973).

4. H. G. Horak and J. W. Kodis, "RADFLO-A User's Manual," Los Alamos National Laboratory report LA-9245-M (in press).

Printed in the United States of America
Available from
National Technical Information Service
US Department of Commerce
5285 Port Royal Road
Springfield, VA 22161

Microfiche (A01)

Page Range	NTIS Price Code	Page Range	NTIS Price Code	Page Range	NTIS Price Code	Page Range	NTIS Price Code
001-025	A02	151-175	A08	301-325	A14	451-475	A20
026-050	A03	176-200	A09	326-350	A15	476-500	A21
051-075	A04	201-225	A10	351-375	A16	501-525	A22
076-100	A05	226-250	A11	376-400	A17	526-550	A23
101-125	A06	251-275	A12	401-425	A18	551-575	A24
126-150	A07	276-300	A13	426-450	A19	576-600	A25
						601-up*	A99

*Contact NTIS for a price quote.

Los Alamos